Global Biogeochemical Cycles

RESEARCH ARTICLE
10.1029/2019GB006396

Key Point:
- Secondary forest in Brazilian Amazon can be highly productive, but frequent disturbances in the region may interrupt the regrowth process

Correspondence to:
Y. Yang,
yangyannn@gmail.com

Citation:
Yang, Y., Saatchi, S., Xu, L., Keller, M., Corsini, C. R., Aragão, L. E. O. C., et al. (2020). Carbon neutrality of secondary forests in the Brazilian Amazon (2004–2014). *Global Biogeochemical Cycles*, *34*, e2019GB006396. https://doi.org/10.1029/2019GB006396

Received 19 AUG 2019
Accepted 3 MAY 2020

Author Contributions:
Conceptualization: Yan Yang, Sassan Saatchi, Liang Xu, Michael Keller, Christianne R. Corsini, Luiz E. O. C. Aragão, Ana P. Aguiar, Yuri Knyazikhin, Ranga B. Myneni
Formal analysis: Yan Yang, Sassan Saatchi, Liang Xu
Writing - original draft: Yan Yang, Sassan Saatchi, Liang Xu

Interannual Variability of Carbon Uptake of Secondary Forests in the Brazilian Amazon (2004-2014)

Yan Yang[1,2], Sassan Saatchi[1,3], Liang Xu[3], Michael Keller[2], Christianne R. Corsini[4], Luiz E. O. C. Aragão[4,5], Ana P. Aguiar[4], Yuri Knyazikhin[2], and Ranga B. Myneni[2]

[1]Institute of Environment and Sustainability, University of California, Los Angeles, CA, USA, [2]Department of Earth and Environment, Boston University, Boston, MA, USA, [3]Jet Propulsion Laboratory, California Institute of Technology, Pasadena, CA, USA, [4]Remote Sensing Division, National Institute for Space Research, São José dos Campos, SP, Brazil, [5]College of Life and Environmental Sciences, University of Exeter, Exeter, UK

Abstract Tropical secondary forests (SF) play an important role in the global carbon cycle as a major terrestrial carbon sink. Here, we use high-resolution TerraClass data set for tracking land use activities in the Brazilian Amazon from 2004–2014 to detect spatial patterns and carbon sequestration dynamics of secondary forests (SF). By integrating satellite lidar and radar observations, we found the SF area in the Brazilian Amazon increased from approximately 22 Mha (10^6 ha) in 2004 to 28 Mha in 2014. However, the expansion in area was also accompanied by a dynamic land use activity that resulted in about 50% recycling of SF area annually from frequent clearing and abandonment. Consequently, the average age of SF remained less than 10 years (age ~8.2 with one standard deviation of 3.2 spatially) over the period of the study. Estimation of changes of carbon stocks shows that SF accumulates approximately 8.5 Mg ha^{-1} year^{-1} aboveground biomass during the first 10 years after clearing and abandonment, 4.5 Mg ha^{-1} year^{-1} for the next 10 years followed by a more gradual increase of 3 Mg ha^{-1} year^{-1} from 20 to 30 years with much slower rate thereafter. The effective carbon uptake of SF in Brazilian Amazon was negligible (0.06 ± 0.03 PgC year^{-1}) during this period, but the interannual variability was significantly larger (± 0.2 PgC year^{-1}). If the SF areas were left to grow without further clearing for 100 years, it would absorb about 0.14 PgC year^{-1} from the atmosphere, partially compensating the emissions from current rate of deforestation in the Brazilian Amazon.

1. Introduction

Tropical forests contain more than a third of global terrestrial carbon pool (Edward T. A. Mitchard, 2018; S. S. Saatchi, Harris, et al., 2011). Over the past four decades, these forests have experienced significant changes from human activities in the form of large-scale deforestation and forest degradation (e.g., logging and fire disturbance) to support agriculture, livestock, and timber industries (Gibbs et al., 2007; Hecht, 2014; Pearson et al., 2017). The estimates of carbon loss from deforestation and land-use change over the last decade vary from 0.8 to 2.9 PgC year^{-1} (Harris et al., 2012; Pan et al., 2011; A. Tyukavina et al., 2015). From all tropical countries, Brazil stands out as the country with largest stock of forest carbon (~23–30% of all pan-tropical countries) (S. S. Saatchi, Harris, et al., 2011) and the largest source of carbon emissions from forest clearing (Hansen et al., 2013; Harris et al., 2012). Despite a signficant effort to reduce more than 70% of carbon emissions from gross deforestation over the past decade (Zarin et al., 2016), the Brazilian Amazon remains the top contributor to total carbon emissions (A. Tyukavina et al., 2015) among tropical countries, mainly due to extensive large-scale logging activities and increased fire frequency from shifting cultivation and clearing for grazing land (Aragão et al., 2014, 2018; Alexandra Tyukavina et al., 2017).

To combat these losses, there has been a major effort in restoring tropical forests through several initiatives such as REDD+ and CBD (Convention on Biological Diversity) among others (Alexander et al., 2011; Sayer et al., 2004). Restoration of secondary forests (SF) is a slow process that can partially offset the rapid loss of carbon from forest clearing through fire (slash and burn) or degradation from timber extraction (Bongers et al., 2015). In most tropical ecosystems, SF regeneration may occur in the absence of any policy incentives through abandonment of actively managed lands (grazing and crop lands) due to socioeconomic drivers such as the decline of commodity price, changes of globalized demands for food production, and migration or urbanization (Hecht & Saatchi, 2007; Olschewski & Benítez, 2005; Rudel et al., 2004). Regardless of the

cause of regeneration, secondary forests can be highly productive, having an average recovery rate of about 3.05 Mg ha^{-1} in the Netotropics, approximately 11–20 times the uptake rate of an old growth forest (Bongers et al., 2015; Poorter et al., 2016). The rate of SF recovery and carbon accumulation, however, depends largely on the history of the land use before abandonment and a suite of environmental factors such as the soil fertility, climate, and the characteristics of regenerating landscape (Banks-Leite et al., 2014; Brown & Lugo, 1990; Johnson et al., 2001, 2001; Poorter et al., 2016; Uhl, 1987). Because of the extent of SF across tropics, the natural regeneration of these forests is widely considered to be an effective low-cost mechanism for carbon sequestration (Chazdon et al., 2016), and SF are often reported as a significant contribution to the global terrestrial carbon sinks (A. R. Houghton & Nassikas, 2018; Pan et al., 2011). Recent research suggests that Neotropical SF take a median time of 66 years to recover about 90% of the original forest carbon (Poorter et al., 2016). Potentially, Neotropical secondary forests may become a large carbon sink, with one estimate of 8.5 PgC in the tropical Latin America over 40 years (Chazdon et al., 2016), where Brazil has the bulk of that carbon sink potential (70%) (Chazdon et al., 2016).

The sequestration potential of SF is estimated through book-keeping models (R. A. Houghton et al., 2015) based on approximate data reported by tropical countries to the Food and Agricutural Organization (FAO). However, these estimates may exaggerate the role of secondary forests for absorbing atmospheric carbon for two reasons: (1) Most tropical countries do not have reliable land use monitoring systems in place and have no data to report on the area of secondary forests, and (2) the reported data do not include the dynamic land use activities of frequent reclearing and regeneration process (Pan et al., 2011). Therefore, considerable uncertainty remains regarding the carbon uptake of SF across global forest ecosystems (Pugh et al., 2019).

In this study, we focus on the carbon sequestration of SF in the Brazilian Amazon because of their large spatial extent and potential contribution to the global carbon balance. Recent studies and observations of the Brazilian Amazon suggest that while SF has been highlighted for its great capacity for carbon sequestration, there is little contribition from SF to the basin-wide carbon sink because of frequent clearing (Davidson et al., 2012). Similarly, the Brazilian national greenhouse gas emission model predicts that secondary regrowth has a small impact on the carbon balance because of the short duration of regeneration before reclearing of the land (Aguiar et al., 2012). Therefore, although the area of SF has increased by a factor of 5 over the period 1978–2002, the mean age of SF predicted from sequestration models remained less than 5 years over the 25-year period (Neeff et al., 2006). However, with more than a decade long decline of deforestation in the Brazilian Amazon in this century (Souza et al., 2013; Alexandra Tyukavina et al., 2017), the fate of SF could change.

Here, we use the spatial distribution of SF areas produced by the TerraClass program from 2004 to 2014 (de Almeida et al., 2016), along with ground, lidar, and radar remote sensing data to quantify the spatial and temporal dynamics of SF in the Brazilian Amazon and its carbon sequestration in the 21st Century. By focusing on the age and carbon accumulation of SF through time series analysis, we show the year-to-year changes of carbon uptake from regeneration and emissions from reclearing process and quantify, for the first time, the contribution of SF carbon sequestration in the Brazilian Amazon for global carbon balance.

2. Materials and Methods

2.1. Materials

2.1.1. Maps of Deforestation and Secondary Forests

We used the deforestation and SF classification maps produced by the National Institute of Space Research (INPE). The deforestation database from the PRODES (Projeto de Monitoramento do Desmatamento na Amazônia Legal por Satélite) project (available at http://bit.ly/1QAp25M) records the time of old-growth forest clearing in the Brazilian Amazon from 1997 to 2016 at 30–60 m spatial resolutions and marks patches of deforestation with at least 6.25 ha in size (Aguilar-Amuchastegui et al., 2014; Hansen et al., 2013; Alexandra Tyukavina et al., 2017). PRODES product does not account for repeated clearing activities at the landscape; that is, for each pixel, the product only records the time of the first deforestation event. This will, therefore, not allow detection of any regeneration once a forest area has been cleared, avoiding any double counting problem.

To decouple deforestation of old-growth forest from deforestation of secondary forests, we used SF classification maps produced and continually updated by the TerraClass project over the Brazilian Amazon.

TerraClass is a complementary project to the PRODES deforestation products that provides detailed information about the land use and forest resurgence in areas cleared from deforestation (de Almeida et al., 2016). The TerraClass products have a 30-m spatial resolution and cover different time periods (2004, 2008, 2010, 2012, and 2014), allowing for statistical analysis of changes of land use and the dynamics of tropical SF areas.

2.1.2. ALOS PALSAR Data

The ALOS (Advance Land Observation Satellite, "DAICHI") PALSAR (Phased Array L-band Synthetic Aperture Radar sensor) Fine-Beam Dual-polarization (FBD) image data with 25 m pixel size after terrain correction and orthorectification were used as the key remote sensing observations to map and monitor forest aboveground biomass (AGB; in Mg ha^{-1}) or carbon (AGC) of SF. L-band Radar (~24 cm wavelength) observations are sensitive to AGB in most forest types globally, where AGB does not exceed 100–150 Mg/ha (Bouvet et al., 2018; E. T. A. Mitchard et al., 2009; S. Saatchi, Marlier, et al., 2011; Yu & Saatchi, 2016). The ALOS PALSAR backscatter products are available globally from a joint project between JAXA and Japan Resources Obervation System Organization over the global forested areas for the periods of 2007–2010, 2015, and 2016 at 25 m spatial resolution. We used ALOS PALSAR mosaic images acquired over the Brazilian Amazon, at HH and HV wave polarization mainly during the dry season when the variations in soil moisture and other environmental conditions were relatively small (Rosenqvist et al., 2007; Shimada et al., 2014). We aggregated the backscatter data to 100-m spatial resolution using spatial averaging, in order to reduce pixel level speckle noise and improve data quality.

2.1.3. GLAS Lidar Data

The spaceborne Geoscience Laser Altimeter System (GLAS) lidar waveform measurements were used in this study as a complementary source for the quantification of forest aboveground biomass. The GLAS sensor aboard the Ice, Cloud and land Elevation Satellite (ICESat) was the first spaceborne waveform sampling lidar instrument to provide measurements of forest height and vertical structure. GLAS emitted short duration laser pulses and recorded the echoes reflected from the Earth's surface (Abshire et al., 2005). Individual non-contiguous samples have an effective resolution of approximately 0.25 ha (varying among lasers) with global sampling (Abshire et al., 2005; Lefsky et al., 2005; Sun et al., 2008). For vegetated surfaces, the return echoes or waveforms from GLAS lidar are the function of canopy vertical distribution of scattering elements (leaves and branches) and ground elevation within the area illuminated by the laser (the footprint), thus reflecting the canopy structure information (Lefsky et al., 2005; S. S. Saatchi, Harris, et al., 2011; Sun et al., 2008).

We used the GLAS/ICESat L2 Global Land Surface Altimetry Data (GLAH14) product and filtered the original data using a series of stringent quality controls and processing steps (Abshire et al., 2005; Mahoney et al., 2014; Sun et al., 2008; Zwally et al., 2014). The first important step is the cloud filter. We selected the GLAS laser pulses only when the quality flag for atmosphere (atm_char_flag) equals to 0 (clear sky). Another issue of GLAS retrieval is signal saturation. Lidar waveforms captured by the GLAS instrument may have pulse distortions when the received energy exceeds the linear dynamic range of GLAS detector. This happens often in areas with flat and bright surfaces. Saturated return signals in forests may not accurately preserve the shape of the scattering elements within canopy. In this study, we removed the saturated GLAS shots by investigating the Saturation Correction Flag. To avoid the false detection of ground and the mixture of signals from both canopy and ground, we also filtered all data with calculated slopes larger than 10°. For the slope calculation, we applied the independent slope method (ISM) by estimating the terrain slope from the GLAS waveform (Mahoney et al., 2014) at each footprint location. The concept of ISM slope calculation relies solely on the GLAS data itself and calculates the ground slope based on the shape of last waveform peak for each lidar shot. The same method has been applied successfully to our other studies related to the Amazon basin (Yang et al., 2018). We estimated GLAS-derived Lorey's Height (LH) as the basal area weighted forest height, for broadleaf forests based on a calibration from ground plots distributed in the Brazilian Amazon (Lefsky, 2010; Lefsky et al., 2005, 2007) for the GLAS observational period from 2003 to 2008.

2.2. Methods

2.2.1. Spatial and Temporal Analysis

We resampled all the raster data sets (TerraClass—30 m; PRODES—30 m/60 m; ALOS—25 m) to grid cells of 100 meters. For our analysis of TerraClass data, we combined three classes, secondary forest, dirty pasture, and regeneration into one class—SF, as they all represent a form of secondary regeneration phase but with

different trajectories of biomass accumulation and dynamics. We developed maps at 100-m (1-ha) with two types of SF pixels: pure SF with 100% of coverage within the pixel and mixed SF with partial coverage of SF from the original 30-m pixel data. For each SF classification map at 100-m spatial resolution, we also produced the accompanied SF fraction map, showing the fraction of SF found in each 100-m pixel. For PRODES product, we used the majority resampling for the aggregation from its original resolution (30–60 m) to 100-m, as the values in PRODES represent the date of deforestation.

The classified SF maps were further analyzed for SF spatial distribution. SF patches in each year with available TerraClass data were calculated using the texture feature of spatial connectivity. We defined an SF patch as the combination of pixels, which are connected to each other. The connectivity only checks the immediate neighbors of the central pixel at the horizontal and vertical directions. This analysis provides information on the distribution of the SF patch size and the spatial extent of activities associated with forest clearing and land abandonment.

2.2.2. Forest Biomass Models

Assuming that the GLAS-estimated Lorey's Height (LH; in meter) at footprint level (~70 m in diameter) can well represent the pixel-level forest canopy at the 100-m spatial resolution, we adopted a well-studied allometric relationship between aboveground biomass (AGB; in Mg ha^{-1}) and LH for the tropical forests in Amazonia that works well from 1-ha to 1 km scale (S. S. Saatchi, Harris, et al., 2011):

$$AGB=0.6011LH^{1.894}, \tag{1}$$

where the coefficients of the model were derived using ground plots distributed in different regions of Amazonia, and the unit of AGB is the weight of aboveground biomass in Mg (10^6 grams) per hectare. The above model assumes that the average wood density (WD) of trees within the plots was approximately 0.6 g cm^{-3}. Although this average value may be suitable for SFs that are distributed in the southern and eastern Amazonia (Ketterings et al., 2001), there will be some uncertainty due to WD variations across the landscape when using equation 1 (S. Saatchi et al., 2015).

Given the GLAS-derived AGB estimates in 2007 and 2008 (overlapped period with ALOS), we extracted the corresponding ALOS HV backscatter data (σ_0) at the same locations for the SF region of TerraClass 2008, coincident with GLAS footprints. We built a parametric model between GLAS-derived AGB (in Mg ha^{-1}) and σ_0 from ALOS PALSAR values (in dB) in the form of log-quadratic function (E. T. A. Mitchard et al., 2009; S. S. Saatchi, Harris, et al., 2011):

$$\sigma_0=exp\left(a+b^{*}ln(AGB)+c^{*}ln(AGB)^2\right), \tag{2}$$

where a, b, and c are the coefficients for the regression function. The fitting process of this regression was only performed over pure SF pixels that have GLAS observations to improve the model accuracy. Due to the saturation effect of Radar data (ALOS) in dense tropical forests, we set an upper threshold (150 Mg/ha) for the AGB model in equation 2; that is, for any backscatter values producing an AGB value larger than 150 Mg/ha according to equation 2, we set AGB to be 150 Mg/ha (Yu & Saatchi, 2016). When biomass reaches 100 Mg/ha (Brown & Lugo, 1990; Wandelli & Fearnside, 2015), radar signal saturation starts to introduce uncertainty in the estimation of biomass in older secondary forests (>10 years). The setting of 150 Mg/ha as a hard threshold of AGB prediction also prevents extreme values due to the exponential form in the model, when the noisy measurement is beyond the model's pseudo-linear range.

The total living carbon density (TCD; in Pg C) of SF was calculated by including the belowground biomass using allometric equation relating to AGB (S. S. Saatchi, Harris, et al., 2011):

$$TCD=0.49F_{sf}\times\left(AGB+0.489AGB^{0.89}\right), \tag{3}$$

where F_{sf} is the area fraction (ranging from 0 to 1) of SF in each 1-ha pixel. Using the TerraClass maps in 2008 and 2010, we created both AGB and TCD maps. Note that we assumed the woody biomass has 49% carbon on a weight/weight basis for all secondary forests (Hartmann et al., 2013). The second term of equation 3 ($BGB = 0.489AGB^{0.89}$) represents below-ground biomass (BGB; in Mg ha^{-1}). Methods for

Table 1
Decision-Tree Based (DTB) Age Quality Assessment (QA) to Estimate Forest Age in 2010. Here, sf04, sf08, and sf10 are the SF Maps in 2004, 2008, and 2010; hv07, hv08, and hv09 are the ALOS HV Values in 2007, 2008, and 2009. "Y" Denotes the Pixel Classified as SF in TerraClass, and "N" Denotes the Pixel Classified as non-SF

sf04	sf08	sf10	hv07	hv08	hv09	PRODES data (age)	Final age
-	N	Y	-	-	<hv08*0.8	≥1	1
-	N	Y	-	-	>hv08*0.8	>1	2
N	Y	Y	-	-	>hv08*0.8	=3	3
N	Y	Y	-	>hv07*0.8	>hv08*0.8	=4	4
N	Y	Y	-	>hv07*0.8	>hv08*0.8	=5	5
N	Y	Y	-	>hv07*0.8	>hv08*0.8	=6	6
Y	Y	Y	-	>hv07*0.8	>hv08*0.8	=7	7
Y	Y	Y		>hv07*0.8	>hv08*0.8	=8	8

collecting belowground biomass data are laborious, time-consuming, and technically challenging to perform correctly. Instead, belowground biomass was usually estimated from aboveground biomass using regression equations developed from field data collected across multiple biomes. A synthesis of data from available literature, along with elimination of data collected using unclear or incorrect methods, provided a universal equation for estimating forest belowground biomass from ~200 field plots (Mokany et al., 2006; S. S. Saatchi, Harris, et al., 2011).

2.2.3. Estimating Age of SF

The estimation of the SF age in our study was initialized by using PRODES data. PRODES product recorded the year of the first deforestation event for each pixel starting from 1997, but it did not record the starting date of forest regeneration or any subsequent deforestation on the land once cleared. Therefore, using PRODES data alone could frequently lead to overestimation of the SF age and thus an erroneous relationship between Age and AGB.

With the availability of ALOS-PALSAR data only from 2007 to 2010, and the TerraClass data starting from 2004, the confirmation of forest age is limited to just a few years. Using PRODES-derived age map in 2010 as the base map, we applied additional corrections by checking values in TerraClass and ALOS HV backscatter and built a decision-tree-based (DTB) age quality assessment (QA) to determine the approximate forest age (Table 1). We started the DTB age QA from an initial guess of forest age using the PRODES-derived data. Secondly, we used TerraClass maps whenever available to check if the age is within reasonable classes (e.g., if a pixel defined by PRODES has an age of 1 or 2 years in 2010, the TerraClass map of 2010 should mark it as SF, whereas the TerraClass 2008 should show as non-SF). Thirdly, we used the PALSAR HV backscatter as an additional check of disturbance. We defined the observable disturbance as, during the period of ALOS observations, HV backscatter of current year being lower than that of previous year by 20% or more. Once disturbance was found, and the forest age determined from previous steps should be incorrect.

2.2.4. Forest Growth Model

To study the relationship between forest age and AGB/Carbon, we selected the pure SF pixels based on the TerraClass 2010 map. Applying the DTB age QA defined above, we obtained eight categories of age classes from 1 to 8 years. The final forest age versus AGB/Carbon relationship was estimated using the median AGB (in Mg ha^{-1}) values for ages (in years) from 1 to 8 years, in the form of the nonlinear Chapman-Richard growth function (Orihuela-Belmonte et al., 2013):

$$Age = A \times ln\left(1 + \alpha AGB^{\beta}\right), \tag{4}$$

where A, α, and β are the coefficients to fit for the nonlinear relationship. We also validated our growth function using field-measured estimates (Marín-Spiotta et al., 2007; Poorter et al., 2016) for forest ages of 10, 20, and 30. Combining equations 2, 3, and 4, we can generate the representative forest age map directly from ALOS HV imagery acquired over the Brazilian Amazon. The ALOS PALSAR prediction of forest age from AGB estimation ignores the variations in the growth pathways (Poorter et al., 2016) by assuming an average growth trajectory. We acknowledge that the choice of the average growth trajectory may introduce large uncertainty for determining forest age at the pixel level. However, the estimates of SF age across the entire region will provide us with a mean history of forest biomass accumulations without the the detailed knowledge of land use history, soil productivity, and climate conditions (Brown & Lugo, 1990; Poorter et al., 2016). For any studies interested in accurate mapping of forest age at the landscape scales, models with explicit representation of other confounding factors must be considered (Chazdon, 2003; Neeff & dos Santos, 2005; Wandelli & Fearnside, 2015). The main methodology used in this study for AGB and Age estimations was summarized in Figure 1.

2.2.5. Uncertainty in Biomass Estimation

The errors associated with the pixel-level GLAS-derived AGB model (σ_{pix}) have the following components (Chen et al., 2015):

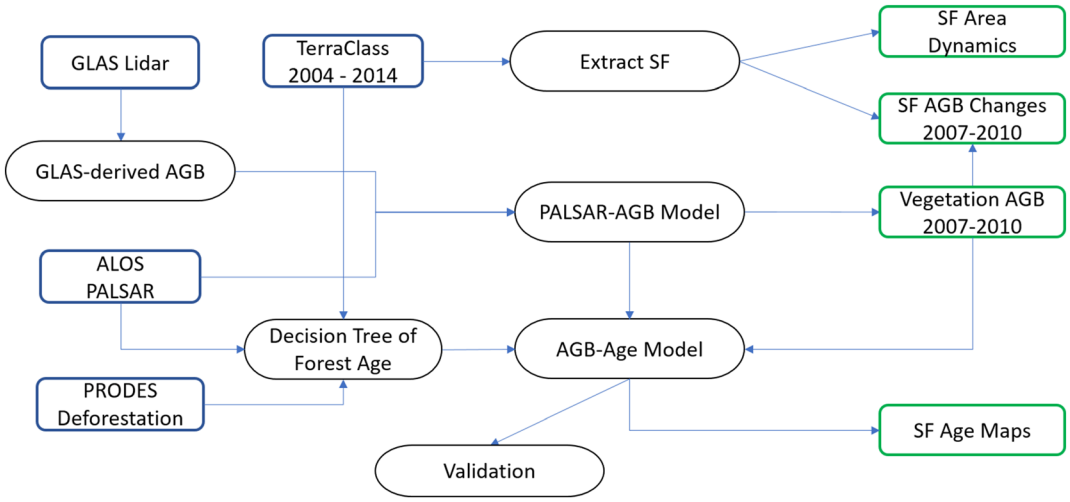

Figure 1. Flow chart summarizing the methodology proposed in this study estimating secondary-forest biomass and age. In the chart, the blue rectangular boxes denote input data, the black rounded boxes are proposed models and data processing, and the green rectangular boxes refer to output products.

$$\sigma_{pix}^2 = \sigma_{\varepsilon,pix}^2 + \sigma_{f,pix}^2 + \sigma_{z,pix}^2, \tag{5}$$

where $\sigma_{\varepsilon,pix}^2$ is the residual variance from the regression model and often modeled as the relative contribution to predicted values so as to account for heteroscedasticity; $\sigma_{f,pix}^2$ is the error variance of predictions associated with model parameters; and $\sigma_{z,pix}^2$ is the error associated with measured lidar metrics. According to the original paper using this model (S. S. Saatchi, Harris, et al., 2011), the residual error of tropical forest could reach ~30% of AGB prediction. Because of the lack of plot-level samples used in the original paper and the associated error assessment of independent variable (Lefsky, 2010), we estimated both variance terms $\sigma_{f,pix}^2$ and $\sigma_{z,pix}^2$ as 16% of AGB prediction (Chen et al., 2015), and thus, the total pixel-level relative AGB prediction error could be ~38%. Our ALOS-PALSAR AGB model (equation 2) was developed based on the GLAS observations, suggesting that the new AGB model inherits the 38% relative AGB error in the new $\sigma_{\varepsilon,pix}^2$ term and enlarges the pixel-level AGB prediction errors. Applying equation 5 to the inversion form of equation 2, we can approximate the propagated error of our AGB estimation.

Uncertainty calculation of regional mean AGB needs to consider the covariance of estimated errors. When different sources of errors are assumed independent, the error variance of regional mean can be expressed as

$$\overline{\sigma}^2 = \frac{1}{N^2}\left(\sum_{i=1}^{N}\sum_{j=1}^{N}\mathrm{cov}\left(\sigma_{\varepsilon,i},\sigma_{\varepsilon,j}\right)\right) + \frac{1}{N^2}\left(\sum_{i=1}^{N}\sum_{j=1}^{N}\mathrm{cov}\left(\sigma_{f,i},\sigma_{f,j}\right)\right) + \frac{1}{N^2}\left(\sum_{i=1}^{N}\sum_{j=1}^{N}\mathrm{cov}\left(\sigma_{z,i},\sigma_{z,j}\right)\right), \tag{6}$$

where the three independent covariance terms are sources of errors related to prediction residuals, model parameters, and input variables (Chen et al., 2016). If the number of pixels is sufficiently large (e.g., our study of SF contains more than 10 million pixels), the regional uncertainty is dominated by the second term, $\overline{\sigma}_f^2$ (Chen et al., 2016), which can be approximated using the first-order Taylor expansion (Ståhl et al., 2010),

$$\overline{\sigma}_f^2 = \sum_{p=1}^{m}\sum_{q=1}^{m}\left(\overline{g}_p\mathrm{cov}\left(\varphi_p,\varphi_q\right)\overline{g}_q\right), \tag{7}$$

where p and q are indices of estimated model parameter covariance matrix, $\mathrm{cov}(\varphi_p,\varphi_q)$, along two dimensions; $\overline{g}_p = \frac{1}{N}\sum_{i=1}^{N}\frac{\partial f}{\partial \varphi_p}$ is the mean of first derivative of prediction with respect to the allometric model (equation 2) parameter φ_p; similarly, $\overline{g}_q$ is the mean of the first derivative of prediction with respect to parameter φ_q; and m is the total number of parameters in the allometric model ($m = 3$ in the case of equation 2). Since the error associated with input variable is often assumed independent

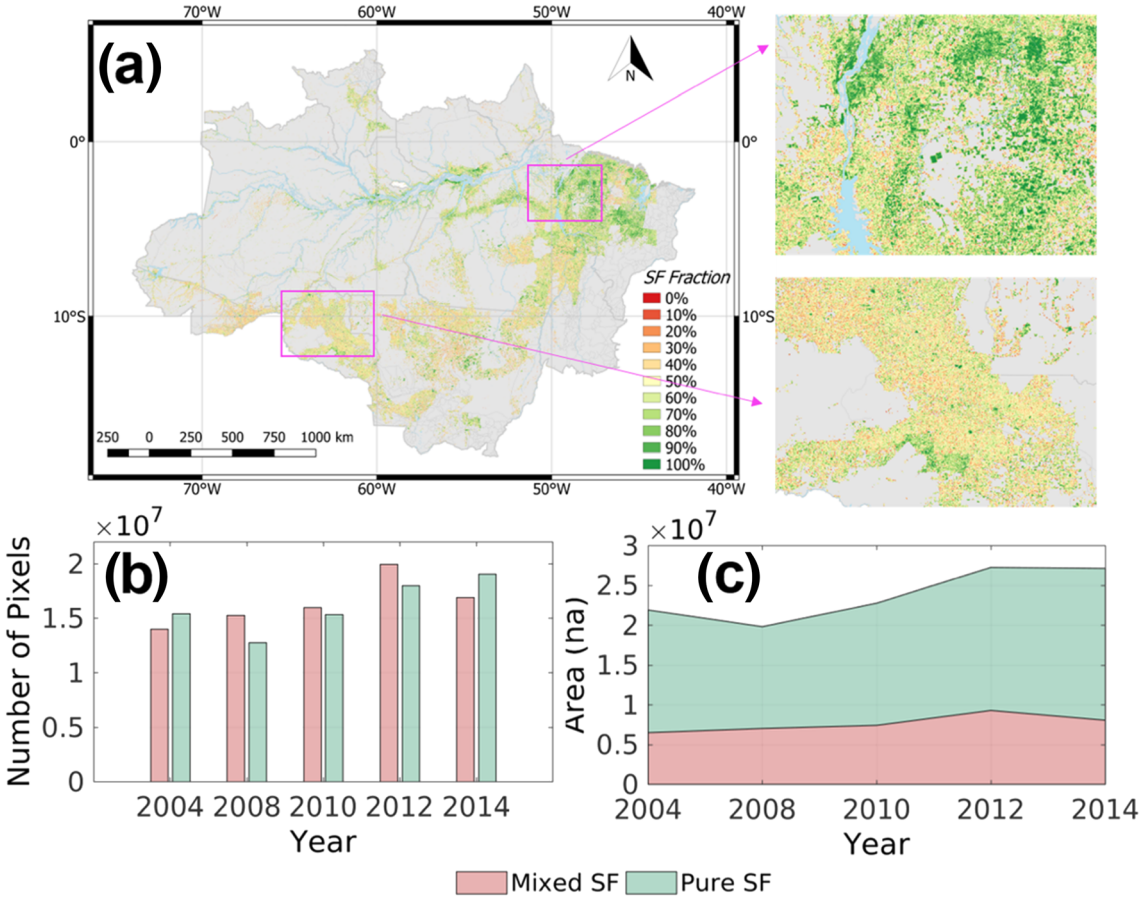

Figure 2. The statistics of secondary forest (SF) in 2004, 2008, 2010, 2012, and 2014. (a) Overview of secondary forest classification map in 2010 (aggregated at 1 km spatial resolution) with zoom-in boxes showing the fraction of SF in different regions; (b) Total number of 1-ha pixels for mixed SF and pure SF for each TerraClass-derived SF map; (c) Total subpixel SF areas present in all pure and in all mixed cells.

of samples, and the residual variance has spatial autocorrelation only within a limited distance, $\overline{\sigma}_f^2$ can explain more than 99% of the error variance for regional estimates over large areas (Chen et al., 2016; Xu et al., 2017). Therefore, even assuming a highly uncertain pixel-level error of ~100% relative to AGB predictions, the regional uncertainty of AGB can still be approximated using equation 7 (Cooke et al., 2016). To avoid numerical errors due to the exponential forms used in the model, we generated multiple sets of model parameters using Monte Carlo simulations based on covariance

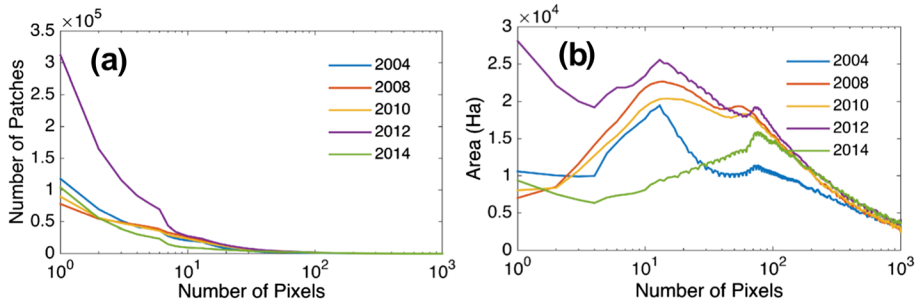

Figure 3. Frequency distribution of SF patches. (a) Number of patches changing with patch size (in terms of number of 1-ha pixels); (b) Associated total area (in hectare) of patches changing with patch size. Different curves correspond to available TerraClass maps in 2004, 2008, 2010, 2012, and 2014.

Table 2
Dynamics of SF Coverage From 2004 to 2014. Gray Cells Show the Total Area of SF in Each Year, Orange Cells Represent the Loss in Coverage From Year A (in Light Green) to Year B (in Light Orange), and Green Cells Denote the New SF Region Gained in Year A (in Light Green), Which Did Not Exist in Year B (in Light Orange)

		Loss (Mha)				
Area (Mha)		2004	2008	2010	2012	2014
Gain (Mha)	2004	21.89	11.32	10.49	10.45	9.57
	2008	9.23	19.80	4.60	8.36	7.75
	2010	11.34	7.54	22.74	9.44	8.60
	2012	15.82	15.82	13.96	27.25	11.67
	2014	14.81	15.08	12.99	11.55	27.13

matrix of parameters and calculated AGB uncertainty from these repeated realizations. We further calculated the regional uncertainty of carbon by adding an additional source of uncertainty from BGB formulation (equation 3) and applied a nominal 20% relative error due to the lack of plot-level data.

The uncertainty of forest growth model (equation 4) can theoretically apply the same uncertainty calculation (equation 5) and propagate errors from AGB modeling. However, the lack of statistical power due to the small sample size in this study could create a large number of type-II errors (Draper & Smith, 1998) and, as a result, making the error assessment of forest age meaningless. Therefore, forest age numbers are reported as nominal values based on limited samples, representing the mean relationship between AGB and Age.

3. Results and Discussion

3.1. Spatial Distribution of SF Area

We estimated the areal coverage of SF over the entire Brazilian Amazon using the TerraClass data. At the 100-m spatial resolution, we found a large fraction of pure SF pixels (12.46 Mha in 2014) in the Eastern Amazon (states of Pará and Maranhão) and a relatively high portion of mixed SF pixels (3.74 Mha in 2014) in the South within states of Rondônia and Mato Grosso. These are regions with frequent land clearing, slash and burn, and small scale land use activities, which together capture a large portion of SF areas (Figure 2a). The mixed SF class has a comparable number of pixels (Figure 2b) to the pure PF pixels but contributes 20%–30% of the total SF area across the Brazilian Amazon (Figure 2c). Therefore, the contribution from mixed SF pixels cannot simply be ignored when reporting the national statistics, and the layer F_{sf}, representing the fraction of SF in each pixel, was kept in the calculation of total carbon density numbers (equation 3).

3.2. Temporal Dynamics of SF Area

The total area of SF in Brazilian Amazon increased by more than 25% from 22 to 28 Mha during the decade from 2004 to 2014 or about 75% from 2002 (16.1 Mha) using earlier Pre-TerraClass estimates (Neeff et al., 2006) (Figure 2c). The increase in the SF area coincides with the reduction in deforestation by more than 50% during this period (Boucher & Chi, 2018).

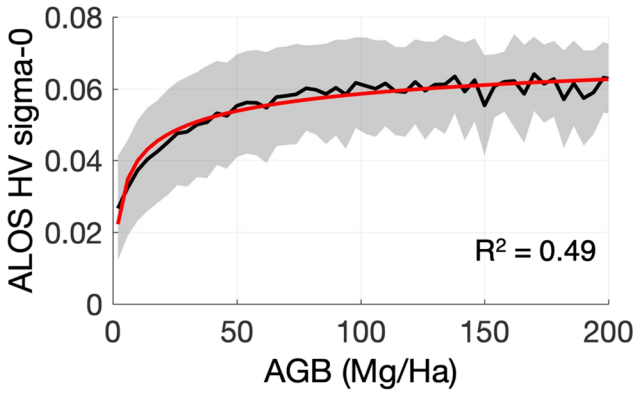

Figure 4. Plot of GLAS-Lidar derived AGB versus ALOS-PALSAR HV backscatter. The solid black line is the mean HV backscatter changing with different AGB ranges (binned for each 10 mg/ha); the shaded area shows one standard deviation of HV backscatter for samples within each AGB bin; and the red line is the fitted model following the form in equation 2. The R^2 value shows the goodness of fit between the fitted line and training samples.

In addition to the area of SF across the Brazilian Amazon, we also explored the SF patch size dynamics using the five (2004, 2008, 2010, 2012, and 2014) TerraClass distribution maps. By defining the patch size as the area of a continguous SF through connected pixels, we explored the frequency distribution of SF patches changing with patch size. Results show that small patches less than 10 ha are the most abundent. The number of patches for each patch size varies year-to-year, particularly for small patches (<10 ha) (Figure 3a). A much higher number of small patches were found in 2012 compared to other years, possibly due to the use of high-resolution ancillary data to compensate the loss of Landsat 5 data. In 2014, we found quite a few small SF patches connected to form relatively large SF patches, significantly changing the distribution of patch sizes from 2012 to 2014. Since small SF patches are more often seen in the Brazilian Amazon (Figure 3a), we also compared the SF coverage (in ha) changing with patch size for different years (Figure 3b). The SF coverage shows a more dynamic distribution of SF areas of different patch sizes, indicating the contributions of small and large patches to the total area of SF are comparable.

The dynamics of SF coverage show that almost half of the existing SF regions changed to other land cover types, and a similar size of forest

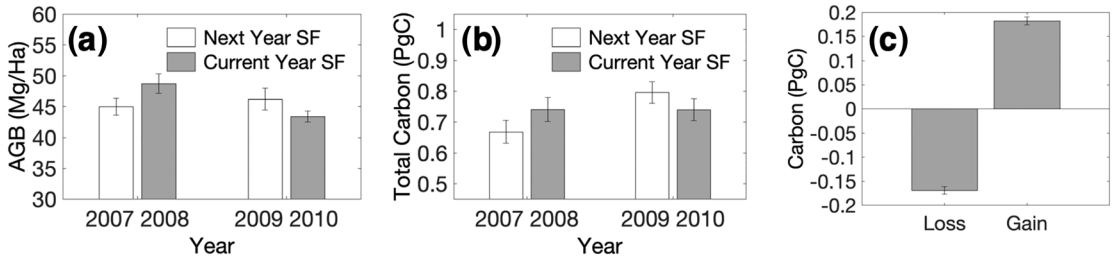

Figure 5. Annual variation of AGB and carbon stock from 2007 to 2010. (a) AGB variations, and (b) total carbon variations. (c) The carbon loss and gain between 2008 and 2010, calculated using SF area loss and gain from Table 2. We used the 2008 SF map to calculate the carbon stock of 2007 and 2008 and the 2010 SF map to calculate the carbon stock of 2009 and 2010. The white boxes thus represent the carbon stock calculation based on the next year's SF maps (e.g., carbon stock of 2007 was calculated using SF of 2008), and the gray boxes represent the carbon stock calcultation using the current year's SF map. The error bar in the figure stands for 95% confidence interval (~2 standard errors) of each mean estimate of AGB or total carbon.

clearing was transformed to SF on a year-to-year basis (Table 2). Although the total area of SF in Brazilian Amazon remains relatively stable through time (varying from 22 to 28 Mha over 10 years), the year-to-year changes suggested frequent clearing of SF areas as part of the land use activities.

3.3. Secondary Forest Biomass

Using GLAS data as the proxy for AGB, we investigated the relationship between AGB and ALOS HV for GLAS samples in 2007 and 2008 that have simultaneous ALOS observations (Figure 4) and translated the backscatter values to AGB by inverting equation 2,

$$AGB = \exp\left(6.52 - 2.83\sqrt{-\sigma^0 - 11.83}\right), \tag{8}$$

where $\sigma^0$is the ALOS PALSAR backscatter data at HV polarization normalized by incidence angle and converted to dB from power ($\sigma^0 = 10 \times log_{10}[Power]$). This parametric model provided us mean AGB estimates over SF regions of Brazilian Amazon from 2007 to 2010. Results show that the mean SF AGB had small but meaningful year-to-year variations from the maximum value of 48.7 ± 0.79 Mg ha^{-1} in 2008 to a minimum value of 43.4 ± 0.44 Mg ha^{-1} in 2010 (Figure 5a). Considering the frequent recycling of SF areas with clearing, our results suggest the net biomass variation in the SF of Brazilian Amazon was small or negligible. Nevertheless, the interannual variability of biomass density can be significant for a few pixels in SF.

Taking both the mixed and pure SF pixels into account based on the SF fractions, we estimated the total carbon in SF for the observational period of ALOS (2007 to 2010) using equation 3. The total carbon stock in SF contributed a small fraction (1.4%) to the total carbon pool (~54 PgC) in the entire Brazilian

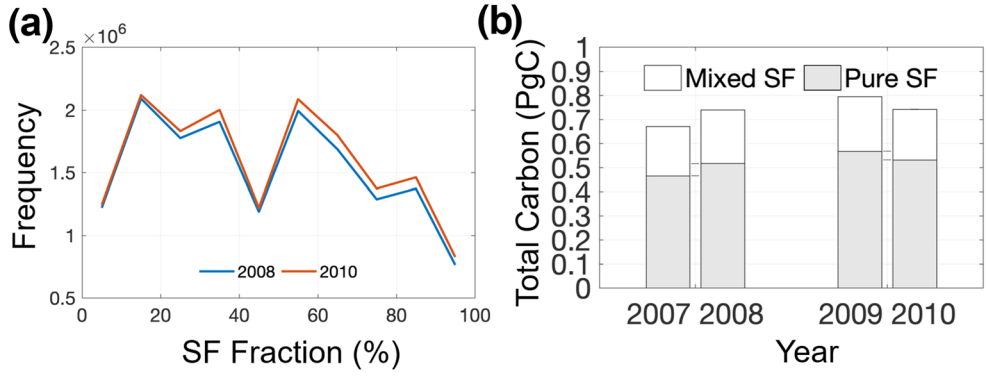

Figure 6. Analysis of mixed SF contribution. (a) Histograms of mixed SF pixels in 2008 and 2010 (pure SF pixels are excluded); (b) annual variations of carbon stock from 2007 to 2010 separating pure and mixed SF pixels. The calculations of total carbon follow the same method used in Figure 5b.

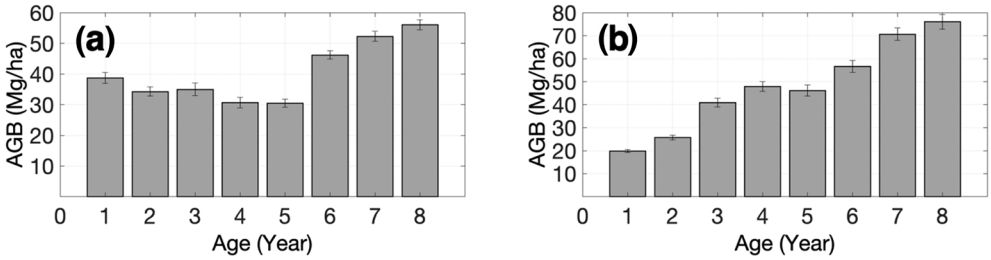

Figure 7. Bar plots showing the relationship between forest age and carbon density (from age 1 to age 8). (a) PRODES SF age map of 2010 without DTB age QA; and (b) SF age map of 2010 with the DTB age QA (see section 2.2.3). The error bar in the figure stands for 95% confidence interval (~2 standard errors) of each mean estimate of AGB.

Amazon (S. S. Saatchi, Harris, et al., 2011). Checking the maximum variation of this carbon pool, we found a significant change from 0.67 ± 0.02 PgC in 2007 to 0.80 ± 0.02 PgC sin 2009 (Figure 5b), translating to an annual carbon sink of 0.06 ± 0.03 PgC year^{-1} in which the increase was mainly due to the change of SF spatial area, as the mean AGB of SF at pixel level had almost no change (Figure 5a). However, the SF spatial areas calculated from TerraClass have their own uncertainties but not evaluated comprehensively. The estimated total carbon of SF in 2010 was in fact lower than the estimation in 2009, probably impacted by the 2010 drought in Amazonia (Lewis et al., 2011; Xu et al., 2011). The seemingly small interannual variability of SF carbon was balanced by the large fractions of gain and loss of SF areas each year. If gain and loss effects were plotted separately, we found a much larger carbon dynamics of around ±0.2 PgC year^{-1} (Figure 5c) in the SF of Brazilian Amazon.

The estimation of AGB and carbon stocks of SF in mixed pixels can be biased due to the use of equation 3 and the mixture of vegetation types occupying these 1-ha pixels. However, the magnitude of this bias, if present, is difficult to quantify. To study the relative importance of the bias and the impact of the mixed pixels on the total carbon stock change of SF, we investigated the distribution of SF fractions during the period of carbon estimations (by comparing the SF maps in 2008 and 2010). Results show that SF fractions had little change from 2008 and 2010 (Figure 6a), indicating any potential biases caused by mixed SF should be small in calculating the carbon fluxes. We also found that the contribution of mixed SF pixels to total carbon never exceeded 30% (Figure 6b), and the dynamics of total carbon from all SF pixels followed the same pattern as of pure SF pixels that dominated (more than 70%) the SF areas.

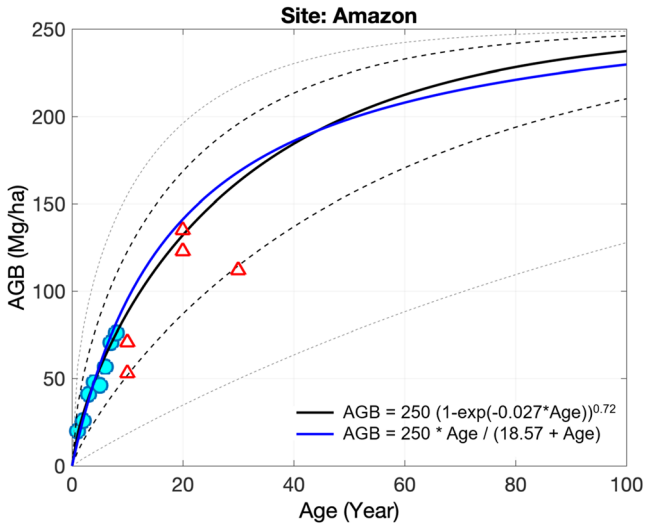

Figure 8. Forest age model showing the relationship between aboveground biomass and age. We used the nonlinear Chapman-Richard growth function of age (Orihuela-Belmonte et al., 2013) (black line). The coefficients are $a = -0.027$ ($-0.046 \sim -0.007$), $b = 0.721$ ($0.473 \sim 0.956$). Numbers in parenthesis show the ranges of 95% confidence intervals. The red triangles are the independent field-measured estimates (Marín-Spiotta et al., 2007; Poorter et al., 2016) for groups of trees at age 10, 20, and 30. Dashed lines show the bounds of one standard error (thick) and 95% confidence interval (thin). We also plotted another popular Age-AGB model from (Batterman et al., 2013) that fits our data (blue line).

3.4. Age-AGB Growth Model of SF

Using equation 4, we converted AGB estimates to forest age. Applying the proposed DTB age QA (Table 1), we show the average distribution of AGB changing with age (Figure 7) across the Brazilian Amazon. Using the median AGB values for ages from 1 to 8, we built the AGB-Age model (in the form of equation 4) for SF forests,

$$Age = -37.55\, ln\left(1 - \left(\frac{AGB}{250}\right)^{1.39}\right), \quad (9)$$

Due to the limited availability of multitemporal SF maps and a short period of ALOS observations, we only tested our model using numbers found in literature for forests older than 8 years of age. Using data based on plot measurements, we found the biomass of SF for ages 10, 20, and 30 years (Marín-Spiotta et al., 2007; Poorter et al., 2016) was mostly within one standard error of our AGB-Age model (Figure 8). Interestingly, for mean

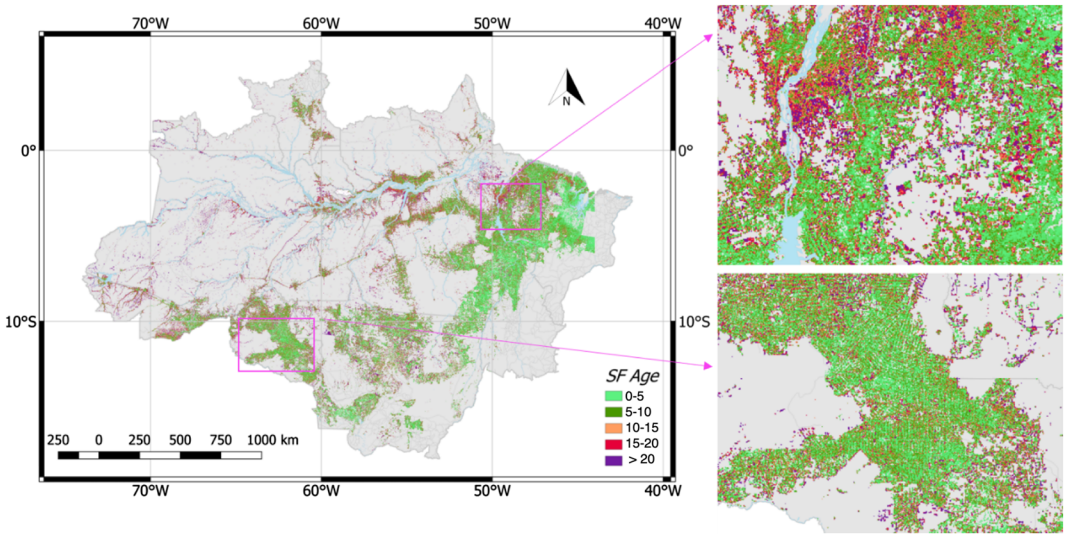

Figure 9. SF age map in 2010 estimated using ALOS backscatter data and AGB-Age model (see SECTION 2.2.4). Zoomed-in images show regions with both old SF and young SF. Note that the AGB-Age model was built from young SF (age < 10 years), and SF ages older than 10 years were inferred from the AGB-Age relationship (Figure 8).

SF biomass at the plot level, Neeff and dos Santos (2005) reported lower values than our model for young forests (age < 10 years). This may have resulted from scaling issues because we estimated biomass at 1-ha grid cells with the possible inclusion of other land-cover types other than secondary forests. Furthermore, the regeneration immediately after the detection of disturbance was included in our estimation from ALOS data but may be absent in other studies. As SF grow older, the plot-level biomass estimation became comparable to other existing estimates.

Regardless of differences in the scale of SF area and biomass estimation, we found a potentially rapid accumulation of forest biomass in SF comparable to other studies (Cassol et al., 2019; Poorter et al., 2016). Our results show that on average, the forests sequestered about 8.5 Mg ha^{-1} year^{-1} during the first 10 years after clearing and abandonment, slowing down to about 4.5 Mg ha^{-1} year^{-1} for the next 10 years, followed by a much gradual growth of about 3 Mg ha^{-1} year^{-1} from the age of 20 to 30 years. These estimates are from average models developed for this study without considering the regional differences and the impacts of soil, climate, and the history of land use.

3.5. Mapping SF Age and Potential Carbon Sink

We estimated the forest age of SF using the AGB-Age model combined with PRODES and TerraClass and with a disturbance correction based on ALOS backscatter (Figure 9). The map shows large areas of young SF (age ≤ 10 years) with the average age of 8.2 years with a standard deviation of 3.2 years, spatially distributed across the entire Brazilian Amazon. Our study predicts a mean SF age within the range of the previous estimations from literature (Carreiras et al., 2017; Cassol et al., 2019; Neeff et al., 2006). However, our study is based on spatial data covering a larger area of secondary forests not sampled in field surveys, and the average age estimate is not old enough to suggest less deforestation or reclearing in SF areas. From the time series analysis and the age maps, we predict that the recycling time of SF in the Brazilian Amazon has been approximately 5 to 10 years. If the 2010 extent of SF (28 Mha) was left to regenerate following the carbon uptake trajectory predicted in this study (Figure 8), the potential SF carbon sink for the region would be about 0.14 PgC year^{-1} over the first 10 years, comparable to the average annual emission quantities from fire or deforestation over the entire Amazon basin (Yang et al., 2018) and significantly larger than the maximum changes of total carbon (Figure 5b) observed in our study.

4. Conclusion

Through the analysis of a suite of satellite data for SF in Brazilian Amazon, we found that young secondary forest is a potentially significant carbon sink because of fast rates of carbon accumulation and rapid expansion of the SF area during the last decade. However, we also found that frequent disturbances of the SF interrupted the regrowth process such that the average SF age never exceeded 10 years. In comparison to intact old growth forests, the SF in the Brazilian Amazon contain a small fraction of the total carbon storage. Moreover, the gain in SF area in recent years translated into only a small sink for carbon annually because the rapid carbon uptake of young SF was balanced by emissions from extensive clearing.

Data Availability Statement

INPE data sets are available online (http://www.inpe.br/cra/projetos_pesquisas/dados_terraclass.php) for TerraClass and (http://www.obt.inpe.br/prodes/index.php) for PRODES. ALOS PALSAR data are available at the website (https://www.eorc.jaxa.jp/ALOS/en/palsar_fnf/fnf_index.htm), and the GLAS/ICESat L2 Global Land Surface Altimetry Data product is available at the website (https://nsidc.org/data/icesat/data.html). Derived SF biomass and age data related to this work are deposited at figshare (https://doi.org/10.6084/m9.figshare.9682046).

Author Contributions

Y.Y. performed data analyses supporting this study. Y.Y., S.S.S., and L.X. designed the study, analyzed data, and wrote the paper. All authors contributed with ideas, writing, and discussions.

Conflict of Interest

The authors declare no competing financial interests. Correspondence and requests for materials should be addressed to Y.Y. (yangyannn@gmail.com).

Acknowledgments

The research was partially supported by NASA Terrestrial Ecology grant (WBS: 596741.02.01.01.67) at the Jet Propulsion Laboratory, California Institute of Technology and partial funding to the UCLA Institute of Environment and Sustainability from previous National Aeronautics and Space Administration and National Science Foundation grants.

References

Abshire, J. B., Sun, X., Riris, H., Sirota, J. M., McGarry, J. F., Palm, S., et al. (2005). Geoscience Laser Altimeter System (GLAS) on the ICESat Mission: On-orbit measurement performance. *Geophysical Research Letters*, *32*, L21S02. https://doi.org/10.1029/2005GL024028

Aguiar, A. P. D., Ometto, J. P., Nobre, C., Lapola, D. M., Almeida, C., Vieira, I. C., et al. (2012). Modeling the spatial and temporal heterogeneity of deforestation-driven carbon emissions: The INPE-EM framework applied to the Brazilian Amazon. *Global Change Biology*, *18*(11), 3346–3366. https://doi.org/10.1111/j.1365-2486.2012.02782.x

Aguilar-Amuchastegui, N., Riveros, J. C., & Forrest, J. L. (2014). Identifying areas of deforestation risk for REDD+ using a species modeling tool. *Carbon Balance and Management*, *9*(1), 10. https://doi.org/10.1186/s13021-014-0010-5

Alexander, S., Nelson, C. R., Aronson, J., & Lamb, D. (2011). Opportunities and challenges for ecological restoration within REDD. Retrieved July 25, 2019, from https://onlinelibrary.wiley.com/doi/abs/10.1111/j.1526-100X.2011.00822.x

Aragão, L. E. O. C., Anderson, L. O., Fonseca, M. G., Rosan, T. M., Vedovato, L. B., Wagner, F. H., et al. (2018). 21st century drought-related fires counteract the decline of Amazon deforestation carbon emissions. *Nature Communications*, *9*(1), 536. https://doi.org/10.1038/s41467-017-02771-y

Aragão, L. E. O. C., Poulter, B., Barlow, J. B., Anderson, L. O., Malhi, Y., Saatchi, S., et al. (2014). Environmental change and the carbon balance of Amazonian forests. *Biological Reviews*, *89*(4), 913–931. https://doi.org/10.1111/brv.12088

Banks-Leite, C., Pardini, R., Tambosi, L. R., Pearse, W. D., Bueno, A. A., Bruscagin, R. T., et al. (2014). Using ecological thresholds to evaluate the costs and benefits of set-asides in a biodiversity hotspot. *Science*, *345*(6200), 1041–1045. https://doi.org/10.1126/science.1255768

Batterman, S. A., Hedin, L. O., van Breugel, M., Ransijn, J., Craven, D. J., & Hall, J. S. (2013). Key role of symbiotic dinitrogen fixation in tropical forest secondary succession. *Nature*, *502*(7470), 224–227. https://doi.org/10.1038/nature12525

Bongers, F., Chazdon, R., Poorter, L., & Peña-Claros, M. (2015). The potential of secondary forests. *Science*, *348*(6235), 642–643. https://doi.org/10.1126/science.348.6235.642-c

Boucher, D., & Chi, D. (2018). Amazon deforestation in Brazil: What has not happened and how the global media covered it. *Tropical Conservation Science*, *11*, 194008291879432. https://doi.org/10.1177/1940082918794325

Bouvet, A., Mermoz, S., Le Toan, T., Villard, L., Mathieu, R., Naidoo, L., & Asner, G. P. (2018). An above-ground biomass map of African savannahs and woodlands at 25m resolution derived from ALOS PALSAR. *Remote Sensing of Environment*, *206*, 156–173. https://doi.org/10.1016/j.rse.2017.12.030

Brown, S., & Lugo, A. E. (1990). Tropical secondary forests. *Journal of Tropical Ecology*, *6*(1), 1–32. https://doi.org/10.1017/S0266467400003989

Carreiras, J. M. B., Jones, J., Lucas, R. M., & Shimabukuro, Y. E. (2017). Mapping major land cover types and retrieving the age of secondary forests in the Brazilian Amazon by combining single-date optical and radar remote sensing data. *Remote Sensing of Environment*, *194*(supplement C), 16–32. https://doi.org/10.1016/j.rse.2017.03.016

Cassol, H. L. G., Carreiras, J. M. B., Moraes, E. C., Aragão, L. E. O. C., Silva, C. V. J., Quegan, S., & Shimabukuro, Y. E. (2019). Retrieving secondary Forest aboveground biomass from Polarimetric ALOS-2 PALSAR-2 data in the Brazilian Amazon. *Remote Sensing*, *11*(1), 59. https://doi.org/10.3390/rs11010059

Chazdon, R. L. (2003). Tropical forest recovery: Legacies of human impact and natural disturbances. *Perspectives in Plant Ecology, Evolution and Systematics*, *6*(1-2), 51–71. https://doi.org/10.1078/1433-8319-00042

Chazdon, R. L., Broadbent, E. N., Rozendaal, D. M. A., Bongers, F., Zambrano, A. M. A., Aide, T. M., et al. (2016). Carbon sequestration potential of second-growth forest regeneration in the Latin American tropics. *Science Advances*, *2*(5), e1501639. https://doi.org/10.1126/sciadv.1501639

Chen, Q., McRoberts, R. E., Wang, C., & Radtke, P. J. (2016). Forest aboveground biomass mapping and estimation across multiple spatial scales using model-based inference. *Remote Sensing of Environment*, *184*, 350–360. https://doi.org/10.1016/j.rse.2016.07.023

Chen, Q., Vaglio Laurin, G., & Valentini, R. (2015). Uncertainty of remotely sensed aboveground biomass over an African tropical forest: Propagating errors from trees to plots to pixels. *Remote Sensing of Environment*, *160*, 134–143. https://doi.org/10.1016/j.rse.2015.01.009

Cooke, R. M., Saatchi, S., & Hagen, S. (2016). Global correlation and uncertainty accounting. *Dependence Modeling*, *4*(1). https://doi.org/10.1515/demo-2016-0009

Davidson, E. A., de Araújo, A. C., Artaxo, P., Balch, J. K., Brown, I. F., Bustamante, M. M. C., et al. (2012). The Amazon basin in transition. *Nature*, *481*(7381), 321–328. https://doi.org/10.1038/nature10717

de Almeida, C. A., Coutinho, A. C., Esquerdo, J. C. D. M., Adami, M., Venturieri, A., Diniz, C. G., et al. (2016). High spatial resolution land use and land cover mapping of the Brazilian Legal Amazon in 2008 using Landsat-5/TM and MODIS data. *Acta Amazonica*, *46*(3), 291–302. https://doi.org/10.1590/1809-4392201505504

Draper, N. R., & Smith, H. (1998). *Applied regression analysis*, (3rd ed. (3rd, Revised, illustrated ed.)). New York: Wiley. https://doi.org/10.1002/9781118625590

Gibbs, H. K., Brown, S., Niles, J. O., & Foley, J. A. (2007). Monitoring and estimating tropical forest carbon stocks: Making REDD a reality. *Environmental Research Letters*, *2*(4), 045023. https://doi.org/10.1088/1748-9326/2/4/045023

Hansen, M. C., Potapov, P. V., Moore, R., Hancher, M., Turubanova, S. A., Tyukavina, A., et al. (2013). High-resolution global maps of 21st-century Forest cover change. *Science*, *342*(6160), 850–853. https://doi.org/10.1126/science.1244693

Harris, N. L., Brown, S., Hagen, S. C., Saatchi, S. S., Petrova, S., Salas, W., et al. (2012). Baseline map of carbon emissions from deforestation in tropical regions. *Science*, *336*(6088), 1573–1576. https://doi.org/10.1126/science.1217962

Hartmann, D. L., Tank, A., & Rusticucci, M. (2013). IPCC fifth assessment report. In *Climate Change 2013: The Physical Science Basis*, (pp. 31–39). Cambridge, United Kingdom and New York, NY, USA: IPCC AR5.

Hecht, S. B. (2014). Forests lost and found in tropical Latin America: The woodland 'green revolution'. *The Journal of Peasant Studies*, *41*(5), 877–909. https://doi.org/10.1080/03066150.2014.917371

Hecht, S. B., & Saatchi, S. S. (2007). Globalization and Forest resurgence: Changes in Forest cover in El Salvador. *Bioscience*, *57*(8), 663–672. https://doi.org/10.1641/B570806

Houghton, A. R., & Nassikas, A. A. (2018). Negative emissions from stopping deforestation and forest degradation, globally. Retrieved July 25, 2019, from https://onlinelibrary.wiley.com/doi/full/10.1111/gcb.13876

Houghton, R. A., Byers, B., & Nassikas, A. A. (2015). A role for tropical forests in stabilizing atmospheric CO_2. *Nature Climate Change*, *5*(12), 1022–1023. https://doi.org/10.1038/nclimate2869

Johnson, C. M., Vieira, I. C. G., Zarin, D. J., Frizano, J., & Johnson, A. H. (2001). Carbon and nutrient storage in primary and secondary forests in eastern Amazônia. *Forest Ecology and Management*, *147*(2–3), 245–252. https://doi.org/10.1016/S0378-1127(00)00466-7

Ketterings, Q. M., Coe, R., van Noordwijk, M., Ambagau', Y., & Palm, C. A. (2001). Reducing uncertainty in the use of allometric biomass equations for predicting above-ground tree biomass in mixed secondary forests. *Forest Ecology and Management*, *146*(1-3), 199–209. https://doi.org/10.1016/S0378-1127(00)00460-6

Lefsky, M. A. (2010). A global forest canopy height map from the moderate resolution imaging spectroradiometer and the geoscience laser altimeter system. *Geophysical Research Letters*, *37*, L15401. https://doi.org/10.1029/2010GL043622

Lefsky, M. A., Harding, D. J., Keller, M., Cohen, W. B., Carabajal, C. C., Espirito-Santo, F. D. B., et al. (2005). Estimates of forest canopy height and aboveground biomass using ICESat. *Geophysical Research Letters*, *32*, L22S02. https://doi.org/10.1029/2005GL023971

Lefsky, M. A., Keller, M., Pang, Y., De Camargo, P. B., & Hunter, M. O. (2007). Revised method for forest canopy height estimation from Geoscience Laser Altimeter System waveforms. *Journal of Applied Remote Sensing*, *1*(1), 013537–013537–18. https://doi.org/10.1117/1.2795724

Lewis, S. L., Brando, P. M., Phillips, O. L., van der Heijden, G. M. F., & Nepstad, D. (2011). The 2010 Amazon drought. *Science*, *331*(6017), 554–554. https://doi.org/10.1126/science.1200807

Mahoney, C., Kljun, N., Los, S. O., Chasmer, L., Hacker, J. M., Hopkinson, C., et al. (2014). Slope estimation from ICESat/GLAS. *Remote Sensing*, *6*(10), 10051–10069. https://doi.org/10.3390/rs61010051

Marín-Spiotta, E., Silver, W. L., & Ostertag, R. (2007). Long-term patterns in tropical reforestation: Plant community composition and aboveground biomass accumulation. *Ecological Applications*, *17*(3), 828–839. https://doi.org/10.1890/06-1268

Mitchard, E. T. A., Saatchi, S. S., Woodhouse, I. H., Nangendo, G., Ribeiro, N. S., Williams, M., et al. (2009). Using satellite radar backscatter to predict above-ground woody biomass: A consistent relationship across four different African landscapes. *Geophysical Research Letters*, *36*, L23401. https://doi.org/10.1029/2009GL040692

Mitchard, E. T. A. (2018). The tropical forest carbon cycle and climate change. *Nature*, *559*(7715), 527–534. https://doi.org/10.1038/s41586-018-0300-2

Mokany, K., Raison, R. J., & Prokushkin, A. S. (2006). Critical analysis of root: Shoot ratios in terrestrial biomes. *Global Change Biology*, *12*(1), 84–96. https://doi.org/10.1111/j.1365-2486.2005.001043.x

Neeff, T., & dos Santos, J. R. (2005). A growth model for secondary forest in Central Amazonia. *Forest Ecology and Management*, *216*(1–3), 270–282. https://doi.org/10.1016/j.foreco.2005.05.039

Neeff, T., Lucas, R. M., dos Santos, J. R., Brondizio, E. S., & Freitas, C. C. (2006). Area and age of secondary forests in Brazilian Amazonia 1978–2002: An empirical estimate. *Ecosystems*, *9*(4), 609–623. https://doi.org/10.1007/s10021-006-0001-9

Olschewski, R., & Benítez, P. C. (2005). Secondary forests as temporary carbon sinks? The economic impact of accounting methods on reforestation projects in the tropics. *Ecological Economics*, *55*(3), 380–394. https://doi.org/10.1016/j.ecolecon.2004.09.021

Orihuela-Belmonte, D. E., de Jong, B. H. J., Mendoza-Vega, J., Van der Wal, J., Paz-Pellat, F., Soto-Pinto, L., & Flamenco-Sandoval, A. (2013). Carbon stocks and accumulation rates in tropical secondary forests at the scale of community, landscape and forest type. *Agriculture, Ecosystems & Environment*, *171*, 72–84. https://doi.org/10.1016/j.agee.2013.03.012

Pan, Y., Birdsey, R. A., Fang, J., Houghton, R., Kauppi, P. E., Kurz, W. A., et al. (2011). A large and persistent carbon sink in the World's forests. *Science*, *333*(6045), 988–993. https://doi.org/10.1126/science.1201609

Pearson, T. R. H., Brown, S., Murray, L., & Sidman, G. (2017). Greenhouse gas emissions from tropical forest degradation: An underestimated source. *Carbon Balance and Management*, *12*(1), 3. https://doi.org/10.1186/s13021-017-0072-2

Poorter, L., Bongers, F., Aide, T. M., Almeyda Zambrano, A. M., Balvanera, P., Becknell, J. M., et al. (2016). Biomass resilience of Neotropical secondary forests. *Nature*, *530*(7589), 211–214. https://doi.org/10.1038/nature16512

Pugh, T. A. M., Lindeskog, M., Smith, B., Poulter, B., Arneth, A., Haverd, V., & Calle, L. (2019). Role of forest regrowth in global carbon sink dynamics. *Proceedings of the National Academy of Sciences*, *116*(10), 4382–4387. https://doi.org/10.1073/pnas.1810512116

Rosenqvist, A., Shimada, M., Ito, N., & Watanabe, M. (2007). ALOS PALSAR: A pathfinder mission for global-scale monitoring of the environment. *IEEE Transactions on Geoscience and Remote Sensing*, *45*(11), 3307–3316. https://doi.org/10.1109/TGRS.2007.901027

Rudel, K. T., Bates, D., & Machinguiashi, R. (2004). A tropical forest transition? Agricultural Change, out-migration, and secondary forests in the Ecuadorian Amazon. Retrieved July 25, 2019, from https://onlinelibrary.wiley.com/doi/abs/10.1111/1467-8306.00281

Saatchi, S., Marlier, M., Chazdon, R. L., Clark, D. B., & Russell, A. E. (2011). Impact of spatial variability of tropical forest structure on radar estimation of aboveground biomass. *Remote Sensing of Environment*, *115*(11), 2836–2849. https://doi.org/10.1016/j.rse.2010.07.015

Saatchi, S., Mascaro, J., Xu, L., Keller, M., Yang, Y., Duffy, P., et al. (2015). Seeing the forest beyond the trees. *Global Ecology and Biogeography*, *24*(5), 606–610. https://doi.org/10.1111/geb.12256

Saatchi, S. S., Harris, N. L., Brown, S., Lefsky, M., Mitchard, E. T. A., Salas, W., et al. (2011). Benchmark map of forest carbon stocks in tropical regions across three continents. *Proceedings of the National Academy of Sciences*, *108*(24), 9899–9904. https://doi.org/10.1073/pnas.1019576108

Sayer, J., Chokkalingam, U., & Poulsen, J. (2004). The restoration of forest biodiversity and ecological values. *Forest Ecology and Management*, *201*(1), 3–11. https://doi.org/10.1016/j.foreco.2004.06.008

Shimada, M., Itoh, T., Motooka, T., Watanabe, M., Shiraishi, T., Thapa, R., & Lucas, R. (2014). New global forest/non-forest maps from ALOS PALSAR data (2007–2010). *Remote Sensing of Environment*, *155*, 13–31. https://doi.org/10.1016/j.rse.2014.04.014

Souza, J., Siqueira, J. V., Sales, M. H., Fonseca, A. V., Ribeiro, J. G., Numata, I., et al. (2013). Ten-year landsat classification of deforestation and forest degradation in the Brazilian Amazon. *Remote Sensing*, *5*(11), 5493–5513. https://doi.org/10.3390/rs5115493

Ståhl, G., Holm, S., Gregoire, T. G., Gobakken, T., Næsset, E., & Nelson, R. (2010). Model-based inference for biomass estimation in a LiDAR sample survey in Hedmark County, NorwayThis article is one of a selection of papers from extending Forest inventory and monitoring over space and time. *Canadian Journal of Forest Research*, *41*(1), 96–107. https://doi.org/10.1139/X10-161

Sun, G., Ranson, K. J., Kimes, D. S., Blair, J. B., & Kovacs, K. (2008). Forest vertical structure from GLAS: An evaluation using LVIS and SRTM data. *Remote Sensing of Environment*, *112*(1), 107–117. https://doi.org/10.1016/j.rse.2006.09.036

Tyukavina, A., Baccini, A., Hansen, M. C., Potapov, P. V., Stehman, S. V., Houghton, R. A., et al. (2015). Aboveground carbon loss in natural and managed tropical forests from 2000 to 2012. *Environmental Research Letters*, *10*(7), 074002. https://doi.org/10.1088/1748-9326/10/7/074002

Tyukavina, A., Hansen, M. C., Potapov, P. V., Stehman, S. V., Smith-Rodriguez, K., Okpa, C., & Aguilar, R. (2017). Types and rates of forest disturbance in Brazilian legal Amazon, 2000–2013. *Science Advances*, *3*(4), e1601047. https://doi.org/10.1126/sciadv.1601047

Uhl, C. (1987). Factors controlling succession following slash-and-burn agriculture in Amazonia. *Journal of Ecology*, *75*(2), 377–407. https://doi.org/10.2307/2260425

Wandelli, E. V., & Fearnside, P. M. (2015). Secondary vegetation in Central Amazonia: Land-use history effects on aboveground biomass. *Forest Ecology and Management*, *347*, 140–148. https://doi.org/10.1016/j.foreco.2015.03.020

Xu, L., Saatchi, S. S., Shapiro, A., Meyer, V., Ferraz, A., Yang, Y., et al. (2017). Spatial distribution of carbon stored in forests of the Democratic Republic of Congo. *Scientific Reports*, *7*(1), 15030. https://doi.org/10.1038/s41598-017-15050-z

Xu, L., Samanta, A., Costa, M. H., Ganguly, S., Nemani, R. R., & Myneni, R. B. (2011). Widespread decline in greenness of Amazonian vegetation due to the 2010 drought. *Geophysical Research Letters*, *38*, L07402. https://doi.org/10.1029/2011GL046824

Yang, Y., Saatchi, S. S., Xu, L., Yu, Y., Choi, S., Phillips, N., et al. (2018). Post-drought decline of the Amazon carbon sink. *Nature Communications*, *9*(1), 3172. https://doi.org/10.1038/s41467-018-05668-6

Yu, Y., & Saatchi, S. (2016). Sensitivity of L-band SAR backscatter to aboveground biomass of global forests. *Remote Sensing*, *8*(6), 522. https://doi.org/10.3390/rs8060522

Zarin, D. J., Harris, N. L., Baccini, A., Aksenov, D., Hansen, M. C., Azevedo-Ramos, C., et al. (2016). Can carbon emissions from tropical deforestation drop by 50% in 5 years? *Global Change Biology*, *22*(4), 1336–1347. https://doi.org/10.1111/gcb.13153

Zwally, H. J., Schutz, R., Hancock, D., & Dimarzio, J. (2014). GLAS/ICEsat L2 Global Land Surface Altimetry Data (HDF5), Version 34. Boulder, Colorado USA. NASA National Snow and Ice Data Center Distributed Active Archive Center. https://doi.org/10.5067/ICESAT/GLAS/DATA211